Microporous and Mesoporous Materials 234 (2016) 186–195

Contents lists available at ScienceDirect

Microporous and Mesoporous Materials

journal homepage: www.elsevier.com/locate/micromeso

Synthesis of aluminum-containing hierarchical mesoporous materials with columnar mesopore ordering by evaporation induced self-assembly

Mert Kurttepeli [a, 1], Roel Locus [b, 1], Danny Verboekend [b, *], Filip de Clippel [b], Eric Breynaert [b], Johan Martens [b], Bert Sels [b, **], Sara Bals [a, ***]

[a] Electron Microscopy for Materials Science (EMAT), University of Antwerp, Groenenborgerlaan 171, B-2020 Antwerp, Belgium
[b] Centre for Surface Chemistry and Catalysis, KU Leuven, Celestijnenlaan 200F, Bus 2461, B-3001 Heverlee, Belgium

ARTICLE INFO

Article history:
Received 4 May 2016
Received in revised form
1 July 2016
Accepted 4 July 2016
Available online 9 July 2016

Keywords:
Hierarchical mesoporous materials
Aluminosilicates
AAO
EISA
Transmission electron microscopy

ABSTRACT

The incorporation of aluminum into the silica columns of hierarchical mesoporous materials (HMMs) was studied. The HMMs were synthesized by a combination of hard and soft templating methods, forming mesoporous SBA-15-type silica columns inside the pores of anodic aluminum oxide membranes via evaporation induced self-assembly (EISA). By adding Al-isopropoxide to the EISA-mixture a full tetrahedral incorporation of Al and thus the creation of acid sites was achieved, which was proved by nuclear magnetic resonance spectroscopy. Electron microscopy showed that the use of Al-isopropoxide as an Al source for the HMMs led to a change in the mesopore ordering of silica material from circular hexagonal (donut-like) to columnar hexagonal and a 37% increase in specific surface (BET surface). These results were confirmed by a combination of nitrogen physisorption and small-angle X-ray scattering experiments and can be attributed to a swelling of the P123 micelles with isopropanol. The columnar mesopore ordering of silica is advantageous towards the pore accessibility and therefore preferential for many possible applications including catalysis and adsorption on the acid tetrahedral Al-sites.

1. Introduction

Since the discovery of ordered mesoporous silica (OMS) [1], these materials received a lot of attention in the fields of adsorption, separation, drug delivery and catalysis because of their easy synthesis, high specific surface, their high mechanical, thermal and chemical stability and their highly ordered mesopores with very narrow pore size distributions [2–5]. OMS can be synthesized using different strategies (acid, neutral or alkaline synthesis) the pore size, pore wall thickness, silica condensation level and pore orientation can be adjusted by varying the synthesis parameters [6–10]. Especially OMS with the 1D pore orientation like MCM-41 and SBA-15 proved very useful because of their very easy synthesis.

For many applications (catalysis, membrane separations, sensors, etc.) however ordering of the 1D-OMS pores at a macroscopic scale in a thin layer or film is desirable [11]. This way a device is created with easily accessible mesopores available over a large area, in which ideally every mesopore yields a similar performance. Thin OMS films have been formed by sol-gel techniques [12,13] and by evaporation induced self-assembly (EISA) [14,15]. To maximize the functionality of the OMS, a hexagonal pore ordering with columnar pores perpendicular to and thus accessible from the surface of the film is desired. However in films the pores tend to orientate parallel to the surface on which the film is casted [12,13]. To overcome this issue, several techniques have been suggested to enhance the degree of porosity perpendicular to the surface, but many of these techniques are rather laborious involving a large number of steps and exotic chemicals and techniques [11,16–18].

Another attractive method to enhance the OMS 1D-porosity perpendicular to the surface is to confine the synthesis to the pores of anodic aluminum oxide (AAO) membranes, resulting in hierarchical mesoporous materials (HMMs). AAO membranes have straight columnar macropores perpendicular to the surface in

* Corresponding author.
** Corresponding author.
*** Corresponding author.
E-mail addresses: danny.verboekend@kuleuven.be (D. Verboekend), bert.sels@kuleuven.be (B. Sels), sara.bals@uantwerpen.be (S. Bals).
[1] M.K. and R.L. contributed equally.

http://dx.doi.org/10.1016/j.micromeso.2016.07.002
1387-1811/

which silica can be synthesized by sol-gel processes [19], vapour phase processes [20] and EISA [5,21–23]. Ideally, the template micelles in the OMS synthesis align parallel to the surface of the AAO pore wall as would be the case in OMS films. However, apart from this desired columnar hexagonal phase, three other mesopore orderings were observed in HMMs: toric (donut-like) and helical circular hexagonal phases and tubular lamellar phases [5,24–30].

Three main types of applications have been put forward for HMMs [31]. First, they can be used as (part of) a device for the adsorption and extraction of chemicals and (small) proteins or the release of drug components. A second type of application is the use of HMMs as nanoreactors to synthesize metal nanorods, which are isolated by dissolving the HMM after synthesis. A third type of application is the use as a membrane for the separation of molecules or nanoparticles. For all of these applications the accessibility of the mesopore is crucial and thus a columnar hexagonal pore ordering is required. However, in the case of SBA-15-type silica large areas containing predominately columnar hexagonal ordering have not been reported.

Another main drawback of HMMs in many of these applications is that it has thus far only be demonstrated for pure-silica OMS, which are chemically inert. A functionalization with aluminum however is very common in standard mesoporous silica, but has not been reported for OMS included in HMM [32]. When tetravalent Si atoms in tetrahedral positions are replaced by trivalent Al atoms in the silica structure by isomorphous substitution, negatively charged sites are created with Lewis and Brønsted acidity [32], which can also be used as cation exchange sites for precursors of (transition) metal catalysts. These acid or metal functional sites have a vast number of applications [32–34].

To optimize the synthesis of OMS in an efficient manner, it is important to carefully characterize the hierarchical mesoporous materials (HMMs) and to study the connection between different synthesis parameters and the resulting structure. One of the main challenges herein is that HMMs contain only a very small fraction of silica material yielding mesopores with diameters of only a few nanometres. Transmission electron microscopy (TEM) is therefore a valuable technique to investigate the structure of these materials at nanoscale [35–37]. In addition, techniques such as small-angle X-ray scattering (SAXS) and nitrogen physisorption are available, which enables one to obtain more general information, such as the porous properties from such complex materials and the periodicity in the mesoporous phases at a broader perspective.

Here, we introduce an optimized synthesis of HMMs by EISA, integrating aluminum in the silica columns inside the pores of AAO membranes. The use of Al-isopropoxide as an Al source results in the transformation of the mesopore ordering towards a preferential columnar hexagonal mesopore ordering. Both the improved mesopore ordering and the acid Al sites open the door towards more advanced applications for HMMs. The generated materials are characterized using numerous bulk and advanced microscopic techniques, enabling the in-depth assessment of the structure, composition, coordination, morphology, and orientation of the OMS inside the AAO membranes.

2. Experimental procedures

2.1. Evaporation induced self-assembly (EISA)

The EISA-synthesis were adjusted from existing EISA-procedures [28]. 3.0 g of 0.2 M HCl (VWR) solution was mixed with 1.8 g (0.1 mol) of distilled water in a glass bottle. Next, 2.08 g (0.01 mol) of tetraethyl orthosilicate (TEOS, Acros) and 3.95 g (0.086 mol) of ethanol (Fisher) were added to this solution. This mixture was prehydrolyzed at 60 °C for 1 h and then cooled to room temperature. In an additional glass bottle, 0.750 g of pluronic P123 (0.13 mmol, Sigma-Aldrich) was mixed with 11.85 g of ethanol. These two solutions were then mixed with the addition of 42.5 mg LiCl (1 mmol, Fisher). For Al-incorporation into the solutions, the 0.01 mol of TEOS (above mentioned) was replaced by mixtures of TEOS and Al-isopropoxide (AliPO, Acros) with Si/Al molar ratios of 50 and 100. To ensure a full dissolution, the AliPO was added to the HCl–H_2O mixture first and heated overnight at 80 °C. The mixture was cooled to room temperature before TEOS and ethanol were added.

AAO membranes were obtained from Whatman® anodisc membrane discs with diameters of 13 and 47 mm and a thickness of 60 μm. The minimum pore size of the AAO membranes was 200 nm at the filter side (a top layer of few microns) and the back side of the membranes contained pore diameters of about 300 nm. The AAO membranes were placed on Teflon Swagelok® ferrules (¼ in) for easy recuperation after the synthesis with the back side (with ~300 nm pore size) facing upwards. 1 mL and 0.1 mL of the EISA solutions were dropped onto the back side 47 mm and the 13 mm membranes respectively. A schematic representation of the procedure is provided in the supporting information (Fig. S2). From here on the back and the filter side of the membrane are referred as the casting and the non-casting side, respectively. The HMMs were then aged overnight in an oven at 30 °C without controlled relative humidity in contrast to earlier reports [28]. After carefully removing the HMMs from the ferrules, the samples were calcined in two steps: 1°/min to 80 °C (stay 12 h) and then 1°/min to 550 °C (stay 8 h). For simplification, a hierarchical mesoporous material containing SBA-15 in the absence of added aluminum in the synthesis is denoted as HMM-Si. HMMs with a Si/Al ratio of 50 and 100 are denoted as HMM-50 and HMM-100, respectively.

2.2. Characterizations

The casting and non-casting side of the HMMs were characterized using a FEI Quanta scanning electron microscope (SEM) in order to resolve their resulting morphology and pore fillings. A thin layer of carbon (~8–10 nm) was deposited on the samples in order to reduce the charging of the samples during electron beam irradiation. High resolution SEM images were collected from the casting and the non-casting side of the HMMs and from the pulverized HMMs (13 mm) using a Nova NanoSEM 450 (FEI) instrument.

Prior to TEM investigation, dedicated sample preparation was applied to obtain electron transparent TEM samples. Plan-view TEM samples (electron beam parallel with the AAO pores) were prepared by gluing the HMM composite material onto a TEM sample preparation holder with the pores of the HMM facing upwards (see Fig. 1(a)). The first side of the HMM was polished using mechanical grinding until a fine surface was obtained. The same procedure was followed for the other side of the HMM, but mechanical thinning was terminated when a total thickness of ~30 μm was achieved. Further sample thinning was performed in a precision ion polishing system (Gatan Duo Mill 600) until a hole was formed in the center of the sample.

Similarly, cross-section TEM samples were prepared in which the pores of the AAO membrane were perpendicular to the electron beam (see Fig. 1(b)). Initially, two pieces of the HMM composite material were glued (Gatan G1) together with two pieces of glass on both sides. The resulting structure was fixed to a TEM sample preparation holder and both sides were mechanically thinned in a similar manner as explained above, until a thickness of ~30 μm was achieved. Again, further thinning was performed using a precision ion polishing system in order to obtain areas at the tip of the structure that are transparent to electrons.

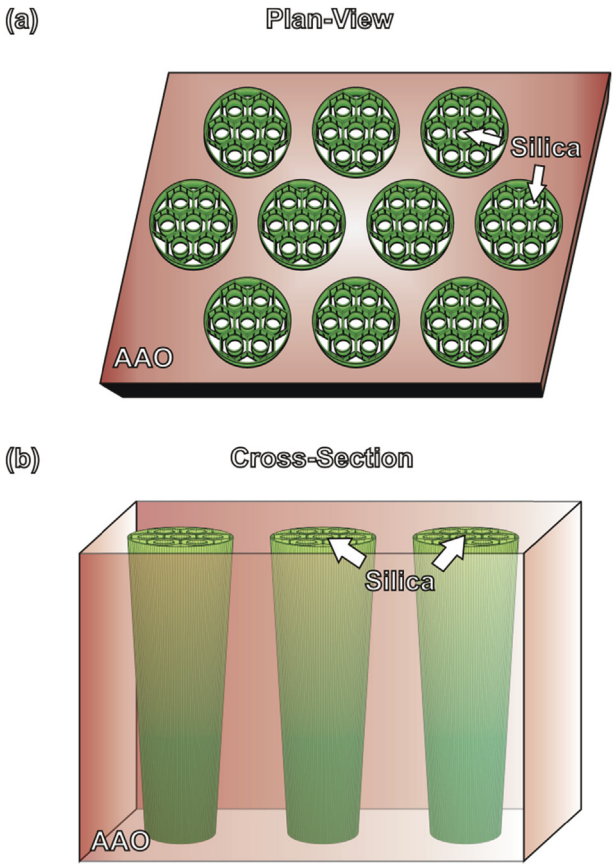

Fig. 1. The schematics represent the orientations of the (a) plan-view and (b) cross-section TEM samples according to the electron beam.

Bright-field TEM (BFTEM), high-angle annular dark field scanning TEM (HAADF-STEM), electron tomography and energy-dispersive X-ray (EDX) elemental mapping were performed using a FEI Tecnai Osiris operated at 200 kV. HAADF-STEM images were recorded using convergence semi-angles in the range of 21–25 mrad with a probe size of approximately 1 Å. Tilt series for electron tomography were acquired by collecting HAADF-STEM images with tilt increments of 2° over a range of ±74° on cross-section TEM samples using an advanced tomography holder from Fischione Instruments. Automated acquisition, alignment and reconstruction of the data using the "Simultaneous Iterative Reconstruction Technique" (SIRT) were carried out using the FEI Inspect3D software package. Amira (Visage Imaging GmbH) was used for the visualization of the reconstructed volume.

The coordination of incorporated Al in the silica was analyzed by ^{27}Al Magic Angle Spinning Nuclear Magnetic Resonance spectroscopy (MAS NMR) using a Bruker Avance 400 spectrometer with a 9.4 T magnet. 12,000 scans are accumulated with a repetition time of 100 ms. The rotor had a spin frequency of 20 kHz. The samples were hydrated for 48 h over a saturated salt solution prior to analysis and packed in a 4 mm MAS rotor.

The N_2 physisorption analysis of the porosity of the pulverized HMMs (47 mm) was carried out using an Autosorb-1 (Quantachrome) instrument at −196 °C. The samples were evacuated for 12 h at 250 °C under vacuum prior to analysis. The specific surface was determined using the BET (Brunauer, Emmett, Teller) model. Pore size distributions (PSDs) were calculated using BJH (Barrett, Joyner, Halenda) and NL-DFT (non-local density functional theory) models.

The periodicity of the mesoporous phases was assessed by measuring Small-Angle X-ray Scattering (SAXS) diffractograms of pulverized 13 and 47 mm HMMs and transmission SAXS patterns of HMMs collected by a SAXSess mc^2 (Anton Paar) instrument illuminated by a line-collimated Cu K_α radiation ($\lambda = 1.54$ Å) and a 2D imaging plate detector.

3. Results

Firstly the Al-incorporation into the HMMs is shortly assessed (Section 3.1), followed by the investigation of the samples with electron microscopy (Sections 3.2 and 3.3). In the next sections the general porous characteristics from nitrogen physisorption and SAXS, respectively, are studied (Sections 3.4 and 3.5), followed by the discussion.

3.1. The incorporation of Al into OMS synthesized by EISA

^{27}Al MAS NMR was used to determine the coordination of the incorporated Al. To increase the Al-signal and to exclude Al from the AAO membrane, the EISA-mixture with a Si/Al-ratio of 50 was dropped into a scale and then aged under the same conditions. The spectrum (Fig. S1) showed a peak located at 60 ppm, a peak at 0 ppm was absent. It is usually presumed that a peak at 60 ppm corresponds to tetrahedrally coordinated Al atoms, incorporated into the silicate walls as desirable framework sites via isomorphous substitution. A peak at 0 ppm indicates octahedrally coordinated Al atoms, which are mostly extra-structure species [32]. Here only a peak at 60 ppm was visible, indicating a complete tetrahedral incorporation of Al into the silica and thus the creation of acid sites (Fig. S1) [32].

3.2. SEM study of the HMMs

The μm-scale morphology of the HMMs was first investigated using SEM. The casting side of the HMMs was often covered with a thin layer of silica, which was in contrast to the non-casting side. Furthermore, SEM analysis showed that the AAO pores on the casting side of the HMMs were filled less frequently with silica in comparison to the non-casting side (Fig. 2(a-b)). On the non-casting side of the HMM (see Fig. 2(b)) a relatively complete filling (90–95%) of the AAO pores is present over a large area. This might be attributed to the movement of the EISA mixture through the pores of the AAO, which can be governed by gravitational and capillary forces. High-resolution SEM analysis of HMM-50 samples additionally indicate the presence of a columnar hexagonal pore ordering in the silica columns (Fig. 2(c-d)).

3.3. In-depth characterization of HMMs using TEM

To assess the effect of Al incorporation in HMMs a more detailed investigation was performed using TEM. In order to image the interior of HMMs, plan-view TEM samples were prepared. A majority of the AAO pores in HMM-50 are filled with columnar hexagonal silica columns (Fig. 3(a)). However, different types of mesopore orderings were observed in the silica columns: a columnar hexagonal ordering (Fig. 3(a) and (c)), a circular hexagonal (donut-like) ordering (Fig. 3(b)) and a combination of the previous two with circular pores on the outside of the silica column and columnar pores in the center (Fig. S3). Also, it should be noted that not all the AAO pores were filled with silica columns. In addition, gaps between the silica columns and the walls of AAO membrane with various sizes are observed independent of the phase of the silica column.

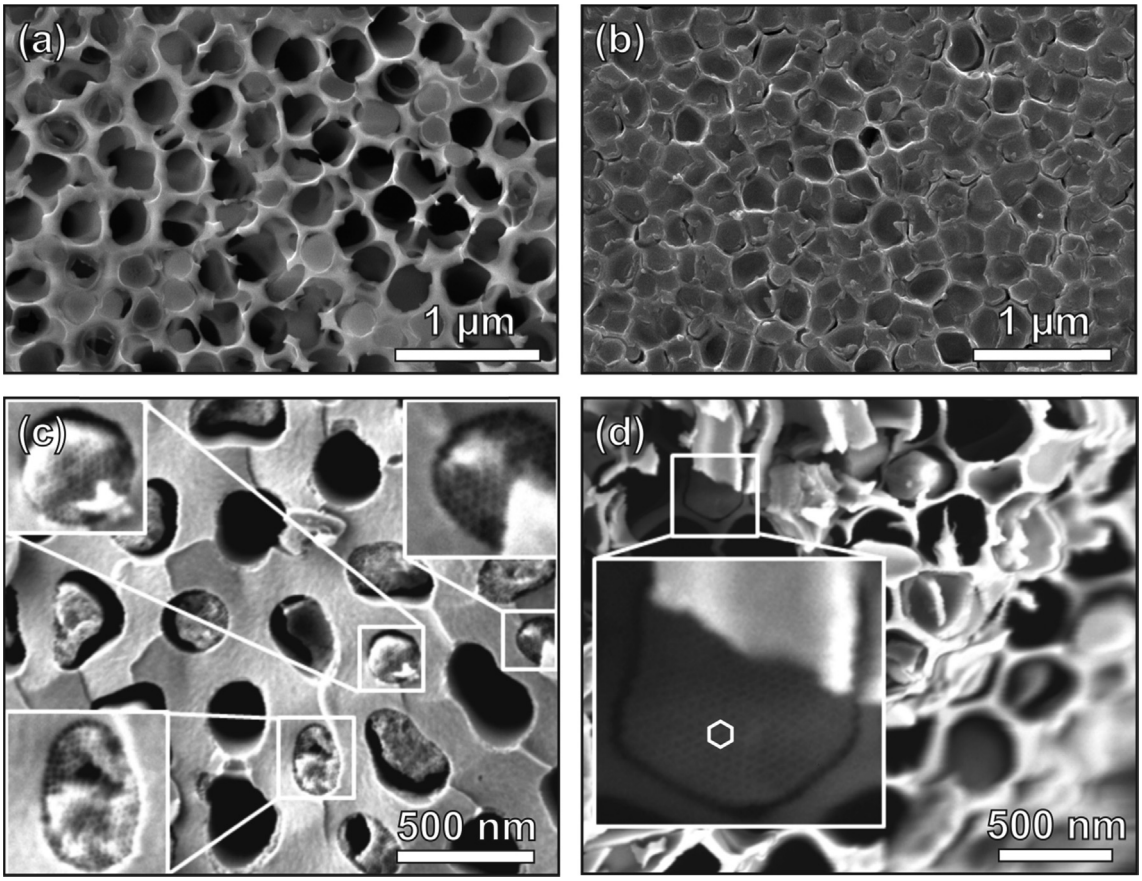

Fig. 2. SEM images of both the casting side (a) and the non-casting side (b) of HMM-50. High-resolution SEM images (c-d) clearly indicate the columnar hexagonal pore ordering in the mesoporous silica columns.

To understand the effect of Al-incorporation on the growth of mesoporous silica inside the pores of AAO membranes, several plan-view TEM samples from HMM-Si, HMM-50 and HMM-100 were prepared and characterized in a quantitative manner as a function of increasing Al content. These results are summarized in Table 1. HMM-Si shows a complete circular hexagonal pore ordering. In HMM-100 and HMM-50 the ratio of the circular hexagonal phase decreased to 0.12 and 0.02 respectively. On the other hand, the ratios of filled AAO pores with a complete columnar hexagonal pore ordering increased from 0 (in HMM-Si) to 0.46 and to 0.63 (in HMM-100 and HMM-50, respectively). Furthermore, the total ratio of filled AAO pores where columnar hexagonal pore ordering is present either partially or completely, does not change substantially for HMM-100 and HMM-50 (varies between 0.61 and 0.69). However, the total ratio of circular hexagonal pore orderings (complete or partial) drops significantly from 0.34 in HMM-100 to 0.08 in HMM-50. Also notable was that HMM-100 contained 35% of the mixed circular-columnar phase (with the circular pores around the central columnar pores as in Fig. S3). It should be kept in mind that not all the AAO pores were filled with silica columns, as mentioned previously. Therefore, this quantification was obtained solely through the characterization of the AAO pores that are filled with the silica columns. After Al-incorporation thus especially the drop in the amount of circular phases was substantial and hence it is suspected that the addition of AliPO to the synthesis inhibits the formation circular phases and promotes the formation of columnar phases without the need to control the relative humidity as was the case in earlier studies [28].

To obtain a complete understanding of the mesopore alignment cross-section TEM samples were investigated. HAADF-STEM reveals that both circular and columnar hexagonal pore orderings occur inside the AAO membranes, but yet the parallel arrangement is most prominent in HMM-50 sample (see Fig. 4). A composition analysis performed by EDX clarifies that the silicon containing columns (silica) are surrounded by the aluminum containing support material (AAO membrane) (insets in Fig. 4). Also the small amount of aluminum present within the silica columns (see Fig. 4(b)) is observed, which confirms that the aluminum in the gel was successfully incorporated in the SBA-15 phase.

In order to incontestably attribute the parallel ordering of mesopores observed with HAADF-STEM to the columnar hexagonal form (Fig. 4(a)), electron tomography is required. Therefore, 3D reconstructions were obtained by electron tomography from the same location where the EDX analysis was performed (Fig. 4(a)). An animated version of the tomogram is provided in the supporting information as a Video. 3D visualizations and the video of the tomogram indicate that the columnar hexagonal pore ordering is present (see Fig. 5(a) and supporting video) along the entire tomography fragment. A slice through the reconstruction is given in Fig. 5(b), which confirms such hexagonal pore ordering parallel to the AAO pores.

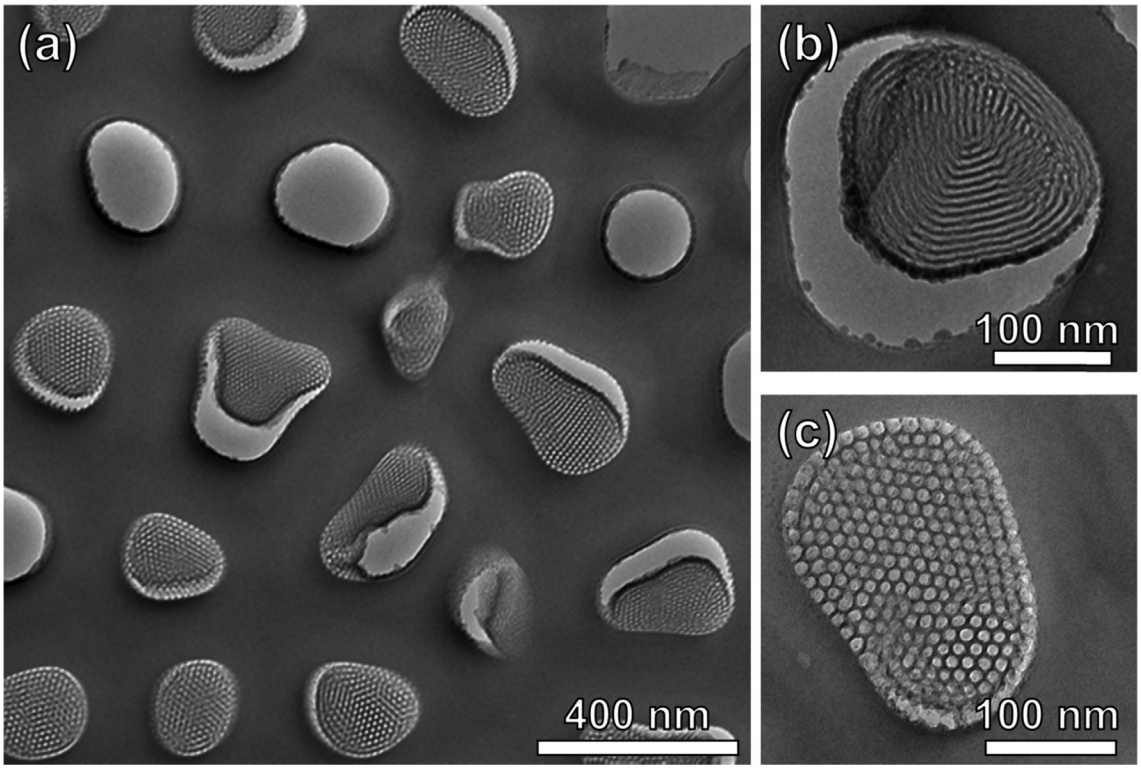

Fig. 3. Plan-view TEM-images (a–c) of HMM-50: (a) general overview showing the good filling of the AAO with columnar hexagonal silica columns. (b-c) More detailed images of the two types of mesoporous orderings: a circular hexagonal ordering (b) and a columnar hexagonal ordering (c).

Table 1
The ratios of the different types of mesopore orderings present in the HMMs.

	HMM-50[a]	HMM-100[b]	HMM-Si[c]
Columnar	0.63	0.46	0
Circular	0.02	0.12	1
Undefined[d]	0.15	0.05	0
Mixed columnar/circular	0.07	0.35	0
Mixed columnar/undefined	0.12	0.02	0
Mixed circular/undefined	0.01	0.00	0
Total columnar	0.69	0.61	0
Total circular	0.08	0.34	1
Total undefined	0.23	0.05	0

[a] 120 filled AAO pores in 19 TEM images were analyzed.
[b] 43 filled AAO pores in 18 TEM images were analyzed.
[c] HMM-Si always showed a complete circular hexagonal mesopore ordering.
[d] Silica phases were denoted undefined when no mesopores were visible.

Supplementary video related to this article can be found at http://dx.doi.org/10.1016/j.micromeso.2016.07.002.

3.4. Study of porosity of the HMMs using N_2 physisorption

Since electron microscopy yields quite local information, N_2 physisorption analysis was used to obtain more average information concerning the porous properties of the HMMs. Fig. 6(a) shows type IV isotherms with hysteresis loops (type H1-H2) indicating capillary condensation in interconnected cylindrical mesopores [38,39]. The hysteresis loop of HMM-Si is markedly broader than the hysteresis loop of HMM-50 especially at lower p/p_0 values. The difference is particularly pronounced in the desorption branch. Fig. 6(b) shows the desorption BJH PSD of the HMMs in which the main peak is visible at 3.9 nm. This peak is almost twice as high in HMM-Si compared to HMM-50. The isotherms and the 3.9 nm peak in the BJH PSD for HMM-100 are intermediate of those from samples HMM-Si and HMM-50 (Fig. S4).

The porosities of the samples are readily correlated to the TEM observations. Since pure silica HMMs consist of circular hexagonal phases, the mesopores in the middle of the HMM are only accessible via smaller interconnecting (micro) pores between the mesopores. Thus lower pressures are required to empty these pores in comparison to the aluminum containing HMMs, giving rise to a more pronounced hysteresis which is also referred to as the ink bottle effect [40–42]. An elegant way to assess this ink bottle effect is by looking at the tensile strength effect (TSE) [39,43]. This is the forced closing of the hysteresis loops in nitrogen isotherms at p/p_0 values of around 0.45, caused by the instability of the nitrogen meniscus in pores smaller than 4 nm. When ink bottle mesopores larger than 4 nm are being blocked by pores smaller than 4 nm the TSE is visible as a sudden kink in the desorption isotherm or as a peak in the BJH PSD at around 4 nm (see Fig. 6). An increasing number of ink bottle pores will lead to a higher the TSE-peak in the BJH PSD. Fig. 6(b) shows the BJH PSD of the HMMs. The TSE-peak of HMM-50 is about half as big as the peak in HMM-Si indicating that HMM-50 has fewer ink bottle mesopores (i.e. circular hexagonal pores).

The PSDs of the HMMs modelled by the NL-DFT can be found in the supporting information and (Fig. S5) are summarized in Table 2. HMM-50 has a pore width of 5.1 nm with tailing to higher values in the equilibrium model and a broad peak around 7.6 nm in the adsorption model (6.7 and 7.6 respectively if weighted mean was calculated). HMM-Si has a pore width of 6.1 nm with tailing to higher values in the equilibrium model and a broad peak around 7.7 nm in the adsorption model (6.9 and 7.7 respectively if weighted mean is calculated). From the sorption experiments also the specific surfaces were calculated with the BET method. For HMM-50, containing mostly columnar hexagonal mesoporous phases, the

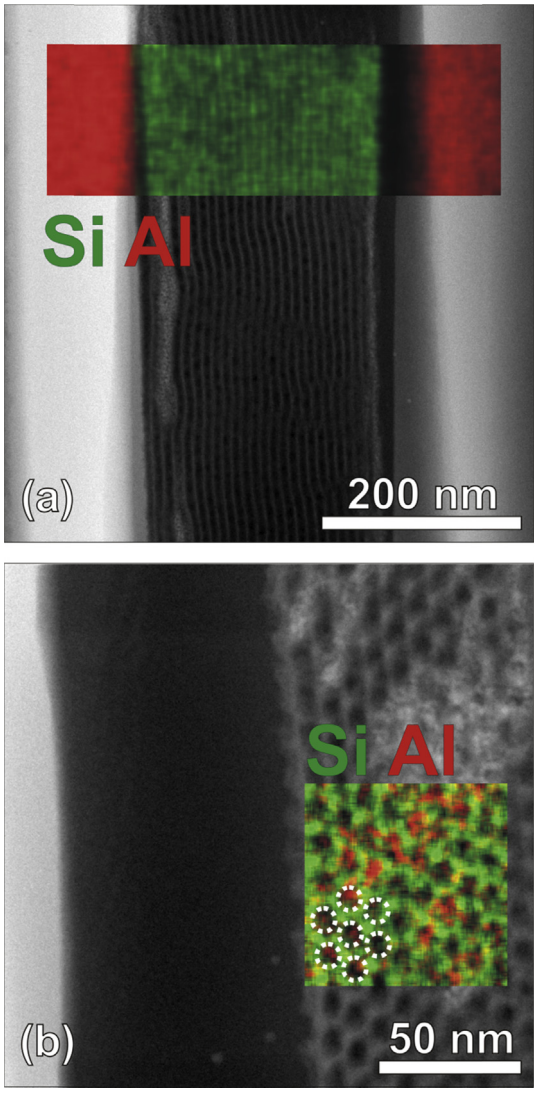

Fig. 4. Cross-sectional HAADF-STEM images reveal the morphology of HMM-50. (a) Shows the columnar hexagonal pore ordering and (b) shows the circular hexagonal pore ordering. The aluminum and the silicon compositions of the sample can be seen on the EDX mixed color elemental maps. (For interpretation of the references to color in this figure legend, the reader is referred to the web version of this article.)

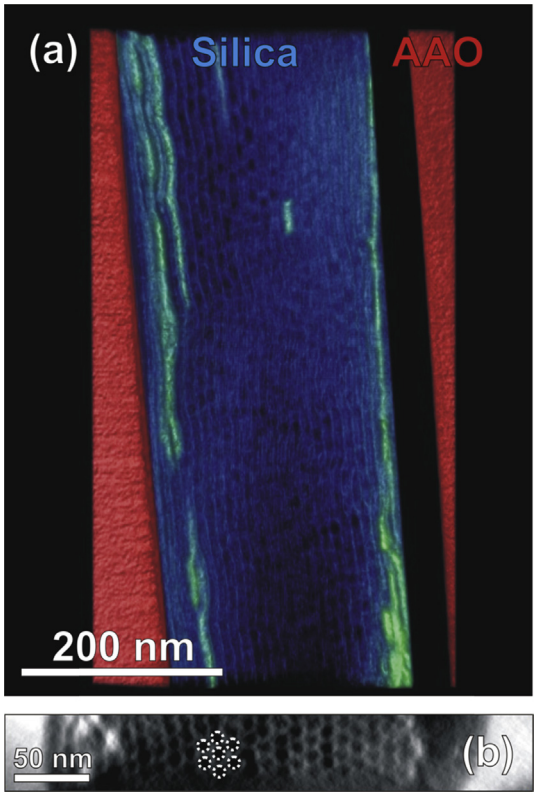

Fig. 5. Electron tomography: (a) Volume rendered 3D visualization of HAADF-STEM reconstructions from HMM-50. (b) A slice through the 3D reconstruction. The hexagonal mesopore ordering is indicated.

equilibrium NL-DFT-model is most suitable, since this model is based on cylindrical pores with a type H1 hysteresis. In HMM-Si, completely made up of circular hexagonal mesoporous phases, the "ink bottle effect" can cause an underestimation of the pore size (larger pores are only emptied at the pressures of lower pores). Desorption based models thus do not give a completely realistic view. Here, the adsorption NL-DFT model for cylindrical pores is most suitable, because it is intended for isotherms with H2 hysteresis (which indicates "ink bottle" pores). Since HMM-50 and HMM-100 contain both phases, the actual PSDs will be a combination of both models. When this is taken into account, it can be concluded that the addition of Al leads to a slight decrease of pore size: 7.6 nm in HMM-Si (adsorption model) to 5.1 nm in HMM-50 (equilibrium model). Compared to the 10.5 nm (equilibrium) and 9.8 nm (adsorption) pore diameters in 100% Si HMM in literature [28], the mesopores of the HMMs synthesized in this research without controlled RH are observed to be smaller. The Al-incorporation is accompanied by an increase in BET-surface of 37% (52 m^2g^{-1} for HMM-Si *vs.* 71 m^2g^{-1} for HMM-50, Table 2), which can partially be explained by the decrease of the pore size in HMM-50. When compared with the 43 m^2g^{-1} BET-surface from the 100% Si HMM from literature [28] the specific surface area of 71 m^2g^{-1} obtained in this research represents a 65% increase in surface area.

3.5. Analysis of the periodicity in the HMM mesophase with SAXS

SAXS was used as a second technique to investigate average properties of the HMMs, i.e. the periodicity in the mesoporous silica phases. Diffractograms were acquired for all HMMs (see Fig. 7(a) and Fig. S6(a)). In order to verify if the large HMMs (47 mm) used for the sorption analysis had the same mesoporous phase as the small (13 mm) HMMs used for SEM and TEM, these were also analyzed with SAXS. A first order (100)-reflection is observed for each HMM sample (Fig. 7(a)). Also a small second order reflection (200) is visible in HMM-Si, which becomes more clear if the diffractograms are divided by the blanco sample (inset in Fig. 7(a)). This reflection is not visible in Al-containing HMMs. Furthermore, the 13 mm and 47 mm HMM-50s show the same reflection A Blanco measurement on AAO membranes filled with amorphous silica shows no reflections since no mesoporous periodicity is present in these samples. The diffractograms converted to d-spacing, show that the addition of Al into the HMMs increases the periodicity distance (d-spacing) from 11.5 nm to 12.5 nm (Fig. 7(b) and Fig. S6(b)).

Second order reflections generally appear when periodicity is present over a larger distance. This can be explained by the fact that the periodicity in columnar hexagonal ordered phases (HMM-50) can only proceed for maximum 300 nm (=AAO pore diameter), because the ordering of the pores is parallel to the AAO pore and

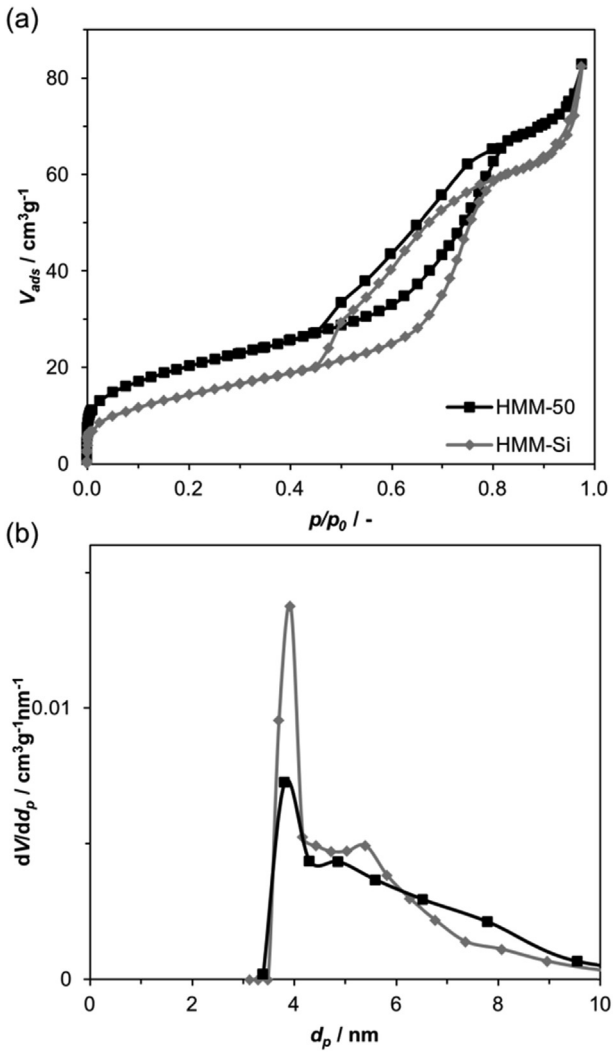

Fig. 6. (a) N_2 physisorption isotherms of HMMs. In HMM-Si a broader hysteresis loop is visible because of the presence of circular hexagonal ink bottle pores. (b) Desorption BJH PSD. The TSE false peak is visible at 3.9 nm. This peak is more pronounced in HMM-Si since more ink bottle pores are present.

concluded that Al-incorporation leads to bigger pore walls. Furthermore the 13 mm and 47 mm HMM-50s showed only little difference and are thus considered to contain the same mesophase.

To compare the HMMs with already existing HMMs in literature, transmissions SAXS experiments were carried out. Both HMM-Si an HMM-50 showed both in-plane and out-of-plane reflections (Fig. S7). The presence of out-of-plane reflections in HMM-50 and HMM-Si showed that both contain a fraction of circular hexagonal ordered mesopores [25]. Since HMM-Si is phase pure (fully circular hexagonal), but HMM-50 contains both circular and hexagonal ordered phases, the SAXS patterns for HMM-Si show more discrete reflections. These results show resemblance with fully circular and mixed circular-columnar P123 samples obtained by Cauda et al. [44].

4. Discussion

The combination of SEM, TEM, N_2 physisorption and SAXS has indicated a shift in mesopore ordering from circular hexagonal to columnar hexagonal after Al incorporation in HMMs. This shift could be attributed to the use AliPO as an Al precursor. After hydrolysis of AliPO isopropanol is present in the EISA solution and it has been reported that this molecule preferentially moves into the hydrophobic part of the P123 micelles as it is relatively hydrophobic [45,46]. Isopropanol thus causes the hydrophobic polypropylene oxide-part of the micelle to swell, making it more difficult to form curved micelles, like the donut shaped micelles, where the concave side is already more densely packed because of the curvature. A more quantitative description can be made by using the formula for the packing parameter (P) of surfactant molecules in a micelle [47]:

$$P = \frac{V}{al}$$

where V is the volume of the hydrophobic tail, a is the interfacial area occupied by the hydrophilic head group and l is the length of the hydrophobic tail. Cylindrical micelles can exist when $0.33 < P < 0.5$. A packing parameter under 0.33 renders spherical micelles [47]. Because of the swelling of tail part with isopropanol, V will increase and thus also P increases. The larger the volume of the tail part is compared to the head group of the surfactant molecule, the harder it is to form (highly) curved cylindrical mi-

Table 2
Summary of the sorption characteristics of HMMs calculated with different models.

Sample	NL-DFT equilibrium model[a] Pore width [nm]	NL-DFT adsorption model[a] Pore width [nm]	BET surface [m^2g^{-1}]
HMM [24]	10.5 (/)[b]	9.8 (/)	43
HMM-Si	6.1 (6.9)[b]	7.6 (7.7)	52
HMM-50	5.1 (6.7)	6.5 (7.6)	71

[a] Pore widths are most frequent values. Weighted mean pore widths are shown in brackets. When the equilibrium model was used, large tailing towards higher values was present and the adsorption model gave broad PSDs (Fig. S5).
[b] Likely underestimated due to cavitation or "ink bottle effects".

thus cannot repeat itself for a distance longer than the AAO pore width. The periodicity in circular hexagonal ordered phases (HMM-Si) is aligned along the AAO pore and thus can be repeated for a longer distance (in theory for 60 μm, i.e. the length of an AAO pore). This longer periodicity distance causes the 2nd order reflection. From the d-space converted results it became clear that the periodicity distance increased from 11,5 nm in HMM-Si to 12,5 nm in HMM-50. When these results are combined with the sorption results (which indicated that HMM-50 had smaller pores), it can be celles (as those present in the circular hexagonal mesophase), because of the increasing steric hindrance at the concave side of the micelle. The curvature of circular micelles near the center of the silica columns is higher than circular micelles close to the AAO pore wall and thus the effect of the isopropanol swelling is higher on these micelles (see Fig. 8). This can be seen in the HMM-100 sample (Fig. S3). The concentration of isopropanol is halved compared to HMM-50 and hence the swelling of the hydrophobic part should be less pronounced. Indeed in HMM-100 35% of the pores were filled

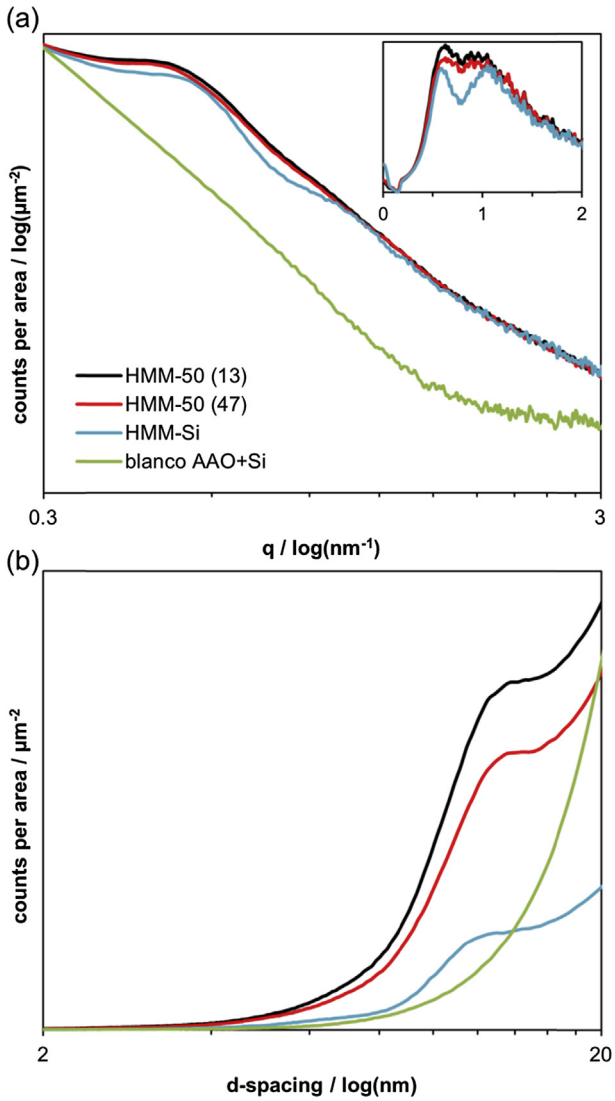

Fig. 7. (a) SAXS diffractograms of HMMs. The HMM-50s only show the first order (100)-reflection. HMM-Si shows a small 2nd order (200)-reflection. The inset shows the diffractograms divided by the blanco sample to accentuate the 2 reflections in HMM-Si. (b) Diffractograms converted to d-spacing, indicating the periodicity distance.

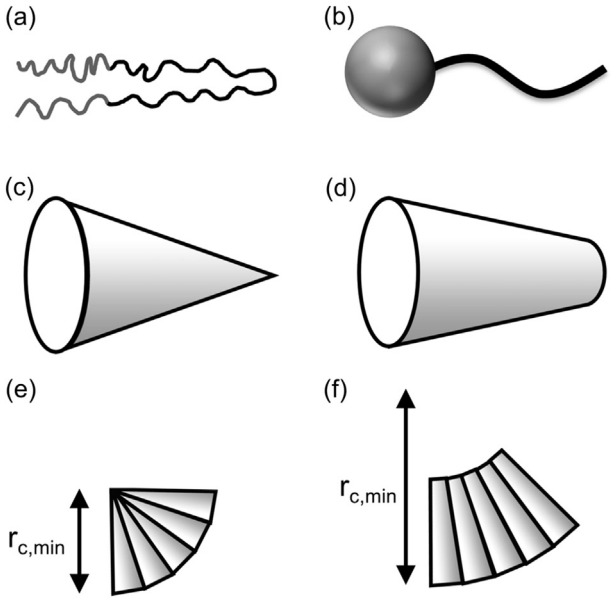

Fig. 8. (a) Schematic representation of the folding of a P123 molecule in a micelle. (b) Schematic representation of a micelle-forming molecule as a hydrophilic head group (grey) and a hydrophobic tail (black). (c,d) (Truncated) cone which is defined by the numbers in the packing parameter formula, wherein 'a' is the area of the base face, 'l' is the height, and 'V' is the volume. After isopropanol swelling (d) the volume of the tail part increases. This swelling implies that minimal radius of curvature ($r_{c,min}$) for the formed micelles increases: (e,f) schematic representation of a part of a micelle without (left) and with (right) swelling.

with a mixed circular-columnar mesophase (circular on the outside of the column, columnar in the center). This means only the formation of the highly curved, circular micelles in the center of the silica columns is inhibited by the isopropanol swelling, but the swelling is not large enough to inhibit the formation of circular micelles on the outside of the silica column, where the curvature is smaller. For HMM-50 the transformation to the columnar mesophase happens in the complete silica column, because of the doubling of the isopropanol concentration and the resulting higher swelling of the hydrophobic micelle part. The addition of AliPO, pure isopropanol, or other additives to the EISA form attractive topics of future study to tune the type and ordering of OMS.

The large increase in the amount of columnar hexagonal mesophases improves the accessibility of the mesopores, which is beneficial for the existing types of applications for the HMM as was stated in the introduction. The incorporation of Al provides a secondary benefit for these applications. The successful incorporation of Al from AliPO in SBA-15 type silica was proven in literature [45] and the ^{27}Al MAS NMR measurements in this research also suggest a full tetrahedral incorporation in the framework (Fig. S1) and thus the presence of acid/charged sites. A first advantage of such sites could be in the adsorption/release applications to improve the specific adsorption of cationic species compared to non-charged or anionic species. Secondly in the formation of metal nanorods, the negative sites could help in assembly of the cationic metal precursors for the nanorods. Finally in membrane applications charged species could be separated easier and a catalysis aspect could be added. An extra advantage is that since the molecules have to pass through the mesopore to go through the membrane a low density of functional sites is needed. The length of the mesopores is approximately 4 orders of magnitude higher than the diameter (see below), which implies frequent collisions of the reagent molecules with the pore walls and thus a high chance of encountering an Al site in the pore wall [48]. In this regard also the incorporation of higher amounts of Al into the HMMs was tested in this research, but this was not possible since the aluminum precipitated during the prehydrolysis step when higher concentrations of AliPO were used. It should be noted that for most applications especially the improved columnar pore ordering is the most important advantage because of the improved accessibility. The high degree of columnar phase we have presented within this contribution has never incontestably been achieved for SBA-15 type HMMs.

An important issue concerning the HMMs that has remained overlooked is the length of the mesopore channels. For many applications and especially towards membranes these pores should be uninterrupted throughout the whole silica column. To observe the continuity (and thus the accessibility) of the mesopores cross-section TEM samples and electron tomography experiments were used. These experiments proved long and continuous columnar mesopores at a micrometer range (see Fig. 5), however the continuity for the full 60 µm of the HMM was not directly shown. Nevertheless an approximate estimation of the length of the mesopores can be made based on the results of this work. Two major

factors will influence the length of the columnar mesopores being the location of the non-columnar impurities and the length of the silica columns. Since the isopropanol swelling suggests that especially the mesopores in the center of the silica columns are converted to the columnar ordering (even in HMM-100), it is expected that the mesopores in the center of the silica columns continue for the largest part of the silica columns. On the other hand it is challenging to predict what occurs at the outside of the columns. Columnar pores near the AAO wall are more likely to be interrupted by occasional circular phases. Concerning the second factor, SEM and TEM suggest that the silica columns fill the majority of the AAO pores, only at the casting side a lesser AAO pore filling was noticed with SEM. SEM and TEM images from the inside of the AAO always contained silica columns, hence the length of the silica columns and also the length of the central columnar mesopores could be around 40–50 μm.

SEM and TEM analysis confirmed the earlier results by Meoto et al. [31] that the challenges remain to synthesize HMMs with all AAO pores filled. The asymmetry observed in this research between casting and non-casting side might partially solve the (incomplete) filling problem. If the HMM would be used as a membrane, it is only important that a small layer of the membrane has a complete filling with the silica columns, here being the non-casting side (Fig. 2(b)). The gaps which were mostly present in the center and the casting side of the HMM thus become insignificant. Concerning these gaps between silica columns and AAO pores, a reported solution is the use of solvents (ethanol/methanol) to extract the surfactant molecules [31]. However the experiments conducted in this research showed that the brittleness of the AAO makes a good stirring of the solvent mixture and the recovery of the HMM without it breaking challenging.

5. Conclusion

The incorporation of aluminum in the ordered mesoporous silica parts of hierarchical mesoporous materials was demonstrated as a valuable tool of enhancing the columnar mesopore ordering and a means to functionalization. Adding Al-isopropoxide to the evaporation induced self-assembly synthesis mixtures led to a complete tetrahedral incorporation of the Al in the silica phase. A combination of electron microscopy techniques proved to be useful in differentiating different pore orientations present in the HMMs. These techniques indicated that the use of AliPO as an Al source caused the mesopore orientation to shift from circular hexagonal to mainly columnar hexagonal, which could be explained by the swelling of the hydrophobic part of the P123 micelles with isopropanol. These results were confirmed by specific features from nitrogen physisorption and small angle X-ray scattering. A combination from the ink bottle effect and the tensile strength effect in the former showed that circular (ink bottle) phases gave rise to a larger TSE peak in the desorption BJH PSD and in the latter circular phases caused 2nd order reflections because of the larger length scale of the periodicity present. The results from this study shed new light on the controlled macroscopic growth of ordered mesoporous silicas, which should be particularly relevant when incorporated in multicomponent devices, such as membranes or as molds for nanorods.

Author contributions

The manuscript was written through contributions of all authors. All authors have given approval to the final version of the manuscript.

Funding sources

The Belgian government (Belgian Science Policy Office, Belspo) is acknowledged for financing the Interuniversity Attraction Poles (IAP-PAI). S. B. acknowledges the financial support from the European Research Council (ERC Starting Grant #335078-COLOURATOMS). D. V. acknowledges the Flanders Research Foundation (FWO).

Acknowledgments

Elke Verheyen is acknowledged for nitrogen physisorption experiments. Sreeprasanth Pulinthanathu is acknowledged for NanoSEM measurements, Kristof Houthoofd is acknowledged for ^{27}Al MAS NMR measurements.

Appendix A. Supplementary data

Supplementary data related to this article can be found at http://dx.doi.org/10.1016/j.micromeso.2016.07.002.

Abbreviations

AliPO	Al-isopropoxide
AAO	anodic aluminum oxide
BET	Brunauer, Emmett, Teller
BJH	Barrett, Joyner, Halenda
EDX	energy-dispersive X-ray
EISA	evaporation induced self-assembly
BFTEM	Bright-field TEM
HMMs	hierarchical mesoporous materials
HAADF-STEM	high-angle annular dark field scanning TEM
OMS	ordered mesoporous silica
NL-DFT	non-local density functional theory
MAS NMR	magic angle spinning nuclear magnetic resonance
PSDs	pore size distributions
SAXS	small-angle X-ray scattering
SEM	scanning electron microscopy
TEM	transmission electron microscopy
TSE	tensile strength effect

References

[1] C.T. Kresge, M.E. Leonowicz, W.J. Roth, J.C. Vartuli, J.S. Beck, Nature 359 (1992) 710–712.
[2] A. Corma, Chem. Rev. 97 (1997) 2373–2420.
[3] J.Y. Ying, C.P. Mehnert, M.S. Wong, Angew. Chem. Int. Ed. 38 (1999) 56–77.
[4] C.-Y. Lai, B.G. Trewyn, D.M. Jeftinija, K. Jeftinija, S. Xu, S. Jeftinija, V.S.Y. Lin, J. Am. Chem. Soc. 125 (2003) 4451–4459.
[5] B. Platschek, A. Keilbach, T. Bein, Adv. Mater. 23 (2011) 2395–2412.
[6] J.S. Beck, J.C. Vartuli, W.J. Roth, M.E. Leonowicz, C.T. Kresge, K.D. Schmitt, C.T.W. Chu, D.H. Olson, E.W. Sheppard, J. Am. Chem. Soc. 114 (1992) 10834–10843.
[7] J.C. Vartuli, K.D. Schmitt, C.T. Kresge, W.J. Roth, M.E. Leonowicz, S.B. McCullen, S.D. Hellring, J.S. Beck, J.L. Schlenker, Chem. Mater. 6 (1994) 2317–2326.
[8] D. Zhao, J. Feng, Q. Huo, N. Melosh, G.H. Fredrickson, B.F. Chmelka, G.D. Stucky, Science 279 (1998) 548–552.
[9] D. Zhao, Q. Huo, J. Feng, B.F. Chmelka, G.D. Stucky, J. Am. Chem. Soc. 120 (1998) 6024–6036.
[10] J. Jammaer, T.S. van Erp, A. Aerts, C.E.A. Kirschhock, J.A. Martens, J. Am. Chem. Soc. 133 (2011) 13737–13745.
[11] A. Walcarius, E. Sibottier, M. Etienne, J. Ghanbaja, Nat. Mater. 6 (2007) 602–608.
[12] Y. Lu, R. Ganguli, C.A. Drewien, M.T. Anderson, C.J. Brinker, W. Gong, Y. Guo, H. Soyez, B. Dunn, M.H. Huang, J.I. Zink, Nature 389 (1997) 364–368.
[13] D. Zhao, P. Yang, N. Melosh, J. Feng, B.F. Chmelka, G.D. Stucky, Adv. Mater. 10 (1998) 1380–1385.
[14] C.J. Brinker, Y. Lu, A. Sellinger, H. Fan, Adv. Mater. 11 (1999) 579–585.
[15] C.J. Brinker, MRS Bull. 29 (2004) 631–640.
[16] V.R. Koganti, S.E. Rankin, J. Phys. Chem. B 109 (2005) 3279–3283.
[17] E.K. Richman, T. Brezesinski, S.H. Tolbert, Nat. Mater. 7 (2008) 712–717.

[18] Z. Teng, G. Zheng, Y. Dou, W. Li, C.-Y. Mou, X. Zhang, A.M. Asiri, D. Zhao, Angew. Chem. Int. Ed. 51 (2012) 2173–2177.
[19] Z. Yang, Z. Niu, X. Cao, Z. Yang, Y. Lu, Z. Hu, C.C. Han, Angew. Chem. Int. Ed. 42 (2003) 4201–4203.
[20] K.J. Lee, S.H. Min, J. Jang, Small 4 (2008) 1945–1949.
[21] A. Yamaguchi, F. Uejo, T. Yoda, T. Uchida, Y. Tanamura, T. Yamashita, N. Teramae, Nat. Mater. 3 (2004) 337–341.
[22] Y. Wu, G. Cheng, K. Katsov, S.W. Sides, J. Wang, J. Tang, G.H. Fredrickson, M. Moskovits, G.D. Stucky, Nat. Mater. 3 (2004) 816–822.
[23] A. Yamaguchi, N. Teramae, Anal. Sci. 24 (2008) 25–30.
[24] B. Platschek, N. Petkov, T. Bein, Angew. Chem. Int. Ed. 45 (2006) 1134–1138.
[25] B. Platschek, R. Köhn, M. Döblinger, T. Bein, Langmuir 24 (2008) 5018–5023.
[26] N. Petkov, B. Platschek, M.A. Morris, J.D. Holmes, T. Bein, Chem. Mater. 19 (2007) 1376–1381.
[27] B. Platschek, R. Köhn, M. Döblinger, T. Bein, ChemPhysChem 9 (2008) 2059–2067.
[28] B. Platschek, N. Petkov, D. Himsl, S. Zimdars, Z. Li, R. Köhn, T. Bein, J. Am. Chem. Soc. 130 (2008) 17362–17371.
[29] A. Keilbach, J. Moses, R. Köhn, M. Döblinger, T. Bein, Chem. Mater. 22 (2010) 5430–5436.
[30] L. Mühlstein, M. Riederer, B. Platschek, T. Bein, J. Mater. Chem. 19 (2009) 9195–9203.
[31] S. Meoto, M.-O. Coppens, J. Mater. Chem. A 2 (2014) 5640–5654.
[32] E. Garrone, F. Fajula, in: H.G. Karge, J. Weitkamp (Eds.), Acidity and Basicity, Springer-Verlag, Berlin Heidelberg, 2008.
[33] A. Corma, D. Kumar, Stud. Surf. Sci. Catal. 117 (1998) 201–222.
[34] D.E. De Vos, M. Dams, B.F. Sels, P.A. Jacobs, Chem. Rev. 102 (2002) 3615–3640.
[35] Z. Gong, G. Ji, M. Zheng, X. Chang, W. Dai, L. Pan, Y. Shi, Y. Zheng, Nanoscale Res. Lett. 4 (2009) 1257–1262.
[36] A. Yamaguchi, H. Kaneda, W. Fu, N. Teramae, Adv. Mater. 20 (2008) 1034–1037.
[37] M. Kurttepeli, S. Deng, S.W. Verbruggen, G. Guzzinati, D.J. Cott, S. Lenaerts, J. Verbeeck, G. Van Tendeloo, C. Detavernier, S. Bals, J. Phys. Chem. C 118 (2014) 21031–21037.
[38] K.S.W. Sing, Pure Appl. Chem. 54 (1982) 2201.
[39] J.C. Groen, L.A.A. Peffer, J. Pérez-Ramırez, Microporous Mesoporous Mater 60 (2003) 1–17.
[40] P. Van Der Voort, P.I. Ravikovitch, K.P. De Jong, A.V. Neimark, A.H. Janssen, M. Benjelloun, E. Van Bavel, P. Cool, B.M. Weckhuysen, E.F. Vansant, Chem. Commun. (2002) 1010–1011.
[41] V.V. Vinogradov, A.V. Agafonov, A.V. Vinogradov, T.I. Gulyaeva, V.A. Drozdov, V.A. Likholobov, J. Sol-Gel Sci. Technol. 56 (2010) 333–339.
[42] P.I. Ravikovitch, A.V. Neimark, Langmuir 18 (2002) 9830–9837.
[43] M.F. De Lange, T.J.H. Vlugt, J. Gascon, F. Kapteijn, Microporous Mesoporous Mater. 200 (2014) 199–215.
[44] V. Cauda, B. Onida, B. Platschek, L. Muhlstein, T. Bein, J. Mater. Chem. 18 (2008) 5888–5899.
[45] A.J.J. Koekkoek, J.A.R. van Veen, P.B. Gerrtisen, P. Giltay, P.C.M.M. Magusin, E.J.M. Hensen, Microporous Mesoporous Mater. 151 (2012) 34–43.
[46] A. Vinu, V. Murugesan, W. Böhlmann, M. Hartmann, J. Phys. Chem. B 108 (2004) 11496–11505.
[47] J. Eastoe, in: T. Cosgrove (Ed.), Colloid Science, Blackwell Publishing Ltd., Oxford, UK, 2009, pp. 50–76.
[48] F. Kapteijn, J.A. Moulijn, G. Emig, R. Dittmeyer, J. Kärger, in: G. Ertl, H. Knözinger, J. Weitkamp (Eds.), Handbook of Heterogeneous Catalysis, Wiley-VCH Verlag GmbH, Weinheim, Germany, 2008, pp. 1189–1261.